Avoiding the Center-Symmetry Trap: Programmed Assembly of Dipolar Precursors into Porous, Crystalline Molecular Thin Films

*Alexei Nefedov, Ritesh Haldar, Zhiyun Xu, Hannes Kühner, Dennis Hofmann, David Goll, Benedikt Sapotta, Stefan Hecht, Marjan Krstić, Carsten Rockstuhl, Wolfgang Wenzel, Stefan Bräse, Petra Tegeder, Egbert Zojer, and Christof Wöll**

Liquid-phase, quasi-epitaxial growth is used to stack asymmetric, dipolar organic compounds on inorganic substrates, permitting porous, crystalline molecular materials that lack inversion symmetry. This allows material fabrication with built-in electric fields. A new programmed assembly strategy based on metal–organic frameworks (MOFs) is described that facilitates crystalline, noncentrosymmetric space groups for achiral compounds. Electric fields are integrated into crystalline, porous thin films with an orientation normal to the substrate. Changes in electrostatic potential are detected via core-level shifts of marker atoms on the MOF thin films and agree with theoretical results. The integration of built-in electric fields into organic, crystalline, and porous materials creates possibilities for band structure engineering to control the alignment of electronic levels in organic molecules. Built-in electric fields may also be used to tune the transfer of charges from donors loaded via programmed assembly into MOF pores. Applications include organic electronics, photonics, and nonlinear optics, since the absence of inversion symmetry results in a clear second-harmonic generation signal.

1. Introduction

Solids with noncentrosymmetric (NC) structure (i.e., those lacking spatial inversion symmetry) exhibit a variety of interesting properties, e.g., piezoelectricity and nonlinear optical (NLO) effects including second-harmonic generation (SHG).[1] Furthermore, the corresponding absence of inversion symmetry is a prerequisite for integrating static electric fields into a material.

A small number of inorganic NC materials exist in nature, e.g., ZnO, KH_2PO_4 (KDP), $LiNbO_3$, and $KTiOPO_4$.[2,3] Recently, artificial inorganic NC compounds[4] have become available through sophisticated deposition processes,[5] which allow to assemble asymmetric (dipolar) subunits into NC structures. This fabrication

Dr. A. Nefedov, Dr. R. Haldar, Z. Xu, B. Sapotta, Prof. C. Wöll
Institute of Functional Interfaces (IFG)
Karlsruhe Institute of Technology (KIT)
Hermann-von-Helmholtz Platz 1
76344 Eggenstein-Leopoldshafen, Germany
E-mail: christof.woell@kit.edu
Dr. R. Haldar
Tata Institute of Fundamental Research Hyderabad
Gopanpally, Hyderabad, Telangana 500046, India
H. Kühner, Prof. S. Bräse
Institute of Organic Chemistry (IOC)
Karlsruhe Institute of Technology (KIT)
Fritz-Haber-Weg 6, 76131 Karlsruhe, Germany
D. Hofmann, D. Goll, Prof. P. Tegeder
Physikalisch-Chemisches Institut
Universität Heidelberg
Im Neuenheimer Feld 253, 69120 Heidelberg, Germany

Prof. S. Hecht
DWI – Leibniz Institute for Interactive Materials
& Institute of Technical and Macromolecular Chemistry
RWTH Aachen University
Forckenbeckstr. 50, 52074 Aachen, Germany
Dr. M. Krstić, Prof. C. Rockstuhl
Institute of Theoretical Solid State Physics (TFP)
Karlsruhe Institute of Technology (KIT)
Fritz-Wolfgang Gaede Str. 1, 76131 Karlsruhe, Germany
Dr. M. Krstić, Prof. C. Rockstuhl, Prof. W. Wenzel
Institute of Nanotechnology (INT)
Karlsruhe Institute of Technology (KIT)
Hermann-von-Helmholtz Platz 1
76344 Eggenstein-Leopoldshafen, Germany
Prof. S. Bräse
Institute of Biological and Chemical Systems (IBCS-FMS)
Karlsruhe Institute of Technology (KIT)
Hermann-von-Helmholtz-Platz 1
76344 Eggenstein-Leopoldshafen, Germany
Prof. E. Zojer
Institute of Solid State Physics
Graz University of Technology
NAWI Graz, Petersgasse 16, Graz 8010, Austria

**ADVANCED
SCIENCE NEWS**
www.advancedsciencenews.com

**ADVANCED
MATERIALS**
www.advmat.de

strategy allowed the integration of electric fields into heterolayered superstructures,[6] which also outperform the natural compounds as regards their NLO properties.

In the field of organic materials, an obvious and straightforward way to obtain NC structures is to use chiral compounds. However, for dipolar building blocks, electrostatic forces prohibit the formation of macroscopic electric fields. Electric fields have been integrated into ultrathin, self-assembled monolayers (SAMs), where organic compounds are anchored to coinage metal substrates via the formation of thiolate bonds.[7] In this case, by using SAM-forming monomers with one or more polar entities incorporated into their backbone, periodic 2D arrays of short dipole stacks have been fabricated.[8] Such strategies are, however, restricted to monolayers and cannot be straightforwardly extended to (hetero) multilayers and thin films. Fabrication methods that break inversion symmetry in assemblies of achiral, dipolar organic molecules to yield a build-up of electric fields are currently underdeveloped compared to methods for inorganic compounds. One rare example is the organic molecular beam deposition of Alq_3 (*tris*(8-hydroxyquinolinate) aluminium (III)).[9] A thorough theoretical analysis revealed a unique compensation of electrostatic interactions by van der Waals forces, which allowed for the build-up of an electrostatic potential.[10]

Generally, for dipolar asymmetric building blocks, electrostatic interactions favor the formation of dimers with antiparallel dipoles, which then aggregate into larger units. This quenching of macroscopic electrostatic fields, occasionally referred to as center-symmetry trap,[1] is a general process in self-assembly of dipolar building blocks[11] prohibiting the formation of NC structures. In selected cases, sophisticated H-bonding schemes have been employed to achieve head-to-tail arrangements with aligned dipoles and interesting electro-optical effects.[12] However, no corresponding supramolecular arrangements into NC crystalline compounds have been reported.

Layer-by-layer (LbL) techniques are among the very few experimental approaches compatible with creating NC structures from asymmetric, achiral organic chromophoric compounds. One example is the Langmuir–Blodgett technique, a method that can be used to transfer molecular monolayers from an air–liquid interface onto a substrate. Such approaches have, indeed been employed for fabricating samples with NLO properties.[13,14] However, sophisticated strategies are often needed to avoid the above-mentioned center-symmetry trap, e.g., by using two different asymmetric monomers.[13] Concerning applications, the necessity of forming monolayers at the air–water interface before transfer, as well as the limited stability of Langmuir–Blodgett films, creates further severe limitations; consequently, built-in electric fields have not yet been reported for this type of layered system. Alternative LbL techniques that have been applied for realizing NC films, e.g., for exploiting first-order nonlinear optics, comprising either sol–gel processes or covalent self-assembly, but none of these approaches affords the realization of porous and crystalline films.[15–20]

The center-symmetry trap also prohibits the integration of static electric fields into molecular heterostructures. Such an engineering of the electrostatic landscape would allow for the experimental realization of structures that have hitherto only been predicted theoretically. This includes dipolar doping[21–23]

and the tuning of band structures at an atomic length scale, which would be required for the fabrication of defined quantum cascades or quantum wells for electrons and holes (e.g., promoting charge carrier separation in solar cells).[24,25]

In multilayers-containing heterojunctions, the inclusion of polar layers would allow switching between Type I and Type II band alignments, as suggested recently for layered semiconductors.[26] Additionally, built-in electric fields could be used to enhance properties of organic light-emitting devices,[27] to promote carrier injection from electrodes or to shift electrostatic energies to a degree that triggers ground-state charge transfer into formerly unoccupied orbitals.[28] This would also allow electrostatic tuning of the electrical conductivity of organic multilayer systems.[29] Finally, anisotropic exciton transport and subsequent separation could be precisely controlled in structures with a bespoke electrostatic landscape, in particular if lateral (parallel to the substrate) gradients could be realized. The particular appeal of realizing porous polar films would be that by filling the pores with functional entities, e.g., organic semiconductors, polar entities, or electron donors and acceptors, one could exploit the change of their properties in the presence of a potential gradient (screening effects notwithstanding).

Here, we overcome previous technical limitations and realize porous, crystalline NC assemblies of dipolar building blocks taking a liquid-phase, quasi-epitaxial LbL approach based on metal–organic frameworks (MOFs).[30] This highly interesting class of crystalline compounds is obtained by connecting suitably functionalized organic compounds (linkers) via metal- or metal–oxo clusters (nodes).[31] While MOFs are conventionally fabricated by one-pot solvothermal methods at elevated temperatures, low-temperature LbL methods have been introduced[32] that allow for the fabrication of multi-heterolayers with compositional gradients directly onto solid substrates.[33] Concerning photonic applications of such surface-mounted MOFs (SURMOFs), a huge variety of appropriate chromophoric linkers has been synthesized, and numerous chromophore-based MOFs and SURMOFs with interesting optical properties have been realized.[34,35] In addition, with regard to lateral patterning of SURMOFs, first results using photo-[36] or electron beam lithography[37,38] have been reported.

Bulk MOF compounds have been fabricated from asymmetric nondipolar subunits to yield NC structures.[22,39,40] To our knowledge, dipolar subunits have not yet been successfully used to assemble MOFs with a macroscopic electrostatic field, although theoretical predictions[41] have indicated the huge potential of such assemblies. Since the ability to produce thin films is a prerequisite for fabricating NC layers with a permanent electric field normal to the surface, we initiated a systematic experimental research effort to reach this goal.

The crucial step in the LbL quasi-epitaxial process for assembling asymmetric MOF linkers into a crystalline structure is to achieve parallel orientation of the dipolar building units. Such an alignment typically does not correspond to the thermodynamic minimum, lattice entropy and electrostatic interactions favor a random, on average anti-parallel alignment of the individual dipoles. To realize fully aligned arrays, we designed ditopic, bifunctional asymmetric MOF linkers that combine a substantial dipole moment with a pronounced asymmetry in the binding energy of the two docking sites. When a suitably
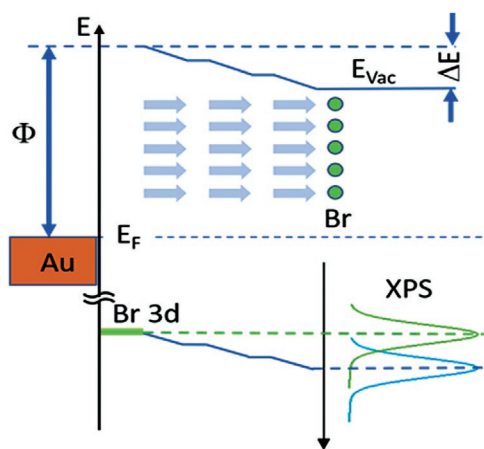
Scheme 1. An illustration of static electric field design using asymmetric subunits in a SURMOF and its effect on Br-core levels (E_F = Fermi energy). The shift of the core levels is caused by a change in electrostatic energy ΔE, which also reduces the work function of the substrate, Φ.

functionalized substrate is exposed to these asymmetric bipyridine units, the latter property enforces that the units first bind with the stronger binding site, thus yielding an oriented adlayer. This process can then be repeated to yield an NC material, as illustrated for a SURMOF in **Scheme 1**. To demonstrate the successful generation of electric fields by this programmed assembly, we monitor the electrostatically induced potential shifts across the entire MOF thin film as a function of the film thickness via recording the Br core-level energies of a correspondingly functionalized top layer (Scheme 1). Furthermore, the NC nature of the fabricated layers is evidenced by the presence of a substantial SHG signal. The observed effects are in full agreement with the results of an extensive set of density functional theory (DFT) calculations.

2. Results and Discussion

The approach presented here is based on a class of MOFs known as the pillared-layer type.[42–44] Briefly, these coordination networks are made with two different types of linkers (see **Figure 1a**). The first type is a ditopic carboxylate linker that creates a 2D network by connecting the paddlewheel-type $(Cu^{2+})_2$ metal nodes. These 2D layers are stacked on top of each other by employing ditopic bipyridine pillars, thus yielding a so-called pillared-layer MOF (see Figure S1, Supporting Information).

In the present work, we chemically modified the pillar linkers to yield asymmetric subunits with a permanent dipole moment. We selected 2,6-dimethyl-4,4′-bipyridine (Me$_2$-BPY) (Figure 1a), which is an asymmetric bipyridine derivative. This ditopic organic compound exhibits a sizeable dipole moment directed toward the substituted ring with a calculated value of 1.0 D. 4,4′-Biphenyldicarboxylic acid was used as the second dicarboxylate linker to construct a pillared-layer Cu(BPDC)(Me$_2$-BPY) SURMOF. To realize an electric field oriented normal to the surface, the 2D layers formed by the paddlewheel node and dicarboxylate linkers must be oriented parallel to the substrate plane, as illustrated in Figure 1a. This was achieved by

functionalizing the corresponding substrates (either Au or sapphire) such that they were terminated by hydroxyl (—OH) groups (see the Experimental Section in the Supporting Information). Previous work has shown that, for this type of substrate functionalization, the growth direction of pillared-layer SURMOFs is along the [001] crystallographic direction, i.e., the axis of the bipyridine units is orientated along the surface normal (Figure 1b).[45]

The methyl-substitution-induced charge redistribution results from the inductive effect of the methyl (–CH$_3$) groups. Importantly, this intramolecular shift of charges not only creates a dipole but also gives rise to substantial differences in the energies that bind the two different pyridine units of the Me$_2$-BPY compound to the Cu paddlewheels. For a single Cu^{2+} ion, this effect would increase the binding energy, but the carboxylate groups of the paddlewheel units cause steric repulsions of the methyl substituent. As a consequence, the nonmodified end of the substituted bipyridine binds more strongly to the Cu-PW unit (see Figure S2, Supporting Information). According to DFT calculations (for details see the Supporting Information), the resulting binding asymmetry amounts to 58 meV, i.e., the calculated binding energy for the dipole-up conformation with the unsubstituted pyridine facing the paddlewheel amounts to 759 meV, while it is only 700 meV for the dipole-down orientation.

As a reference, a nonfunctionalized pillar 4,4′-bipyridine (BPY) was used to grow symmetric Cu(BPDC)(BPY) SURMOFs. In accord with expectation, X-ray diffraction (XRD) data (Figure 1c) revealed that the growth direction was the same as in the case of the asymmetric SURMOF. To determine the presence of electric field gradients (and the corresponding changes in electrostatic energy) within the SURMOFs, a Br-substituted linker (tetrabromoterephthalic acid, Br$_4$-BDC) was attached to the top of the MOF thin film in the last deposition step (see the Experimental Section in the Supporting Information).

All symmetric and asymmetric SURMOFs used in the context of this work were characterized using out-of-plane and in-plane XRD (Figure 1c), as well as IR (see Figure S3, Supporting Information) and X-ray photoelectron (XPS) spectroscopies (see Figure S4, Supporting Information). The XRD results revealed the presence of highly oriented, crystalline MOF thin films with the crystallographic [001] orientation directed perpendicular to the surface, i.e., the pillars were orientated such that their coordination axis was aligned normal to the substrate plane. Scanning electron microscopy (SEM) investigations of the SURMOF cross-sections enabled the determination of the film thickness and the estimation of the surface roughness (Figure S5, Supporting Information).

To demonstrate the presence of built-in electric fields, we determined the XPS core-level shifts of Br marker atoms, an often-used approach in detecting electrostatic gradients at surfaces and in thin films.[46] To be able to determine the overall shift in electrostatic energy across the entire film, the marker atoms were attached only to the outer surface of the symmetric and asymmetric SURMOFs by using tetrabromoterephthalic acid in the last LbL step. For the symmetric Cu(BPDC)(BPY) SURMOFs, the XPS results revealed a core-level binding energy of the Br 3d signal of 72.5 eV, as expected (see the Supporting Information for details of the XPS calibration process using the
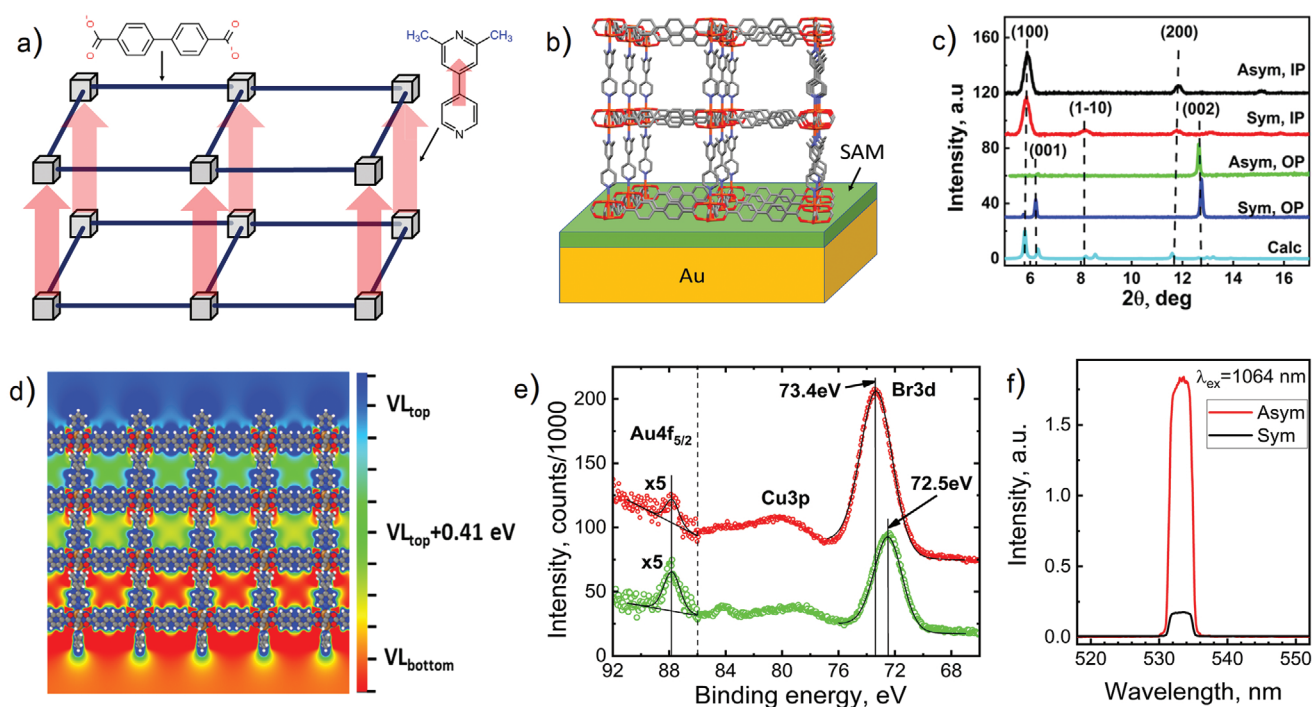
**ADVANCED
SCIENCE NEWS**

www.advancedsciencenews.com

**ADVANCED
MATERIALS**

www.advmat.de

Figure 1. a) A schematic illustration of an NC pillared-layer SURMOF design using an asymmetric pillar. b) Structure of Cu(BPDC)(Me$_2$-BPY) oriented along the [001] direction. c) Simulated (light blue curve) as well as experimental in-plane (IP) and out-of-plane (OP) XRD patterns of asymmetric (Asym) Cu(BPDC)(Me$_2$-BPY) and symmetric (Sym) Cu(BPDC)(BPY) SURMOFs. d) Shift in electrostatic energy for a Cu(BPDC)(Me$_2$BPY) thin film containing three polar Me$_2$BPY apical linker layers. The scale is aligned relative to the vacuum energy below the thin film and is specified relative to the overall change in the vacuum level (VL, calculated as −0.82 eV). e) XPS data recorded for symmetric Cu(BPDC)(BPY) (green circles) and asymmetric Cu(BPDC)(Me$_2$-BPY) (red circles) SURMOFs of 150 nm thickness. Both SURMOFs are coated with a Br$_4$-BDC-containing layer on top. The Gaussian fit of Au 4f$_{5/2}$ and Br 3d peaks with the corresponding background is shown with black lines. f) SHG spectra of the asymmetric Cu(BPDC)(Me$_2$-BPY) and symmetric Cu(BPDC)(BPY) SURMOF were recorded with an excitation wavelength (λ_{ex}) of 1064 nm.

Au 4f signal of the substrate as a reference). In the case of the asymmetric Cu(BPDC)(Me$_2$-BPY) SURMOFs, the Br 3d signal was shifted to higher energies, the maximum observed value amounted to 0.9 eV. The actual values of the binding energy shifts were found to depend on the SURMOF film thickness, as illustrated in the inset of Figure S4 (Supporting Information). A similar XPS-based approach was used earlier to demonstrate the presence of potential gradients originating from oriented dipoles included in the backbone of SAM-forming monomers.[47,48]

The known structure of the Cu(BPDC)(Me$_2$-BPY) SURMOFs allows for a consistent explanation of the observed core-level shifts. Since the binding energy to the Cu paddlewheel secondary building units is larger for the dipole-up orientation (vide supra), we expect the resulting electric field to be oriented such that the electrostatic energy for an electron decreases when moving away from the surface. This increases core-level binding energies, as shown schematically in the bottom panel of Scheme 1. This heuristic expectation is corroborated by DFT calculations of the electrostatic energy for a hypothetical free-standing SURMOF containing three oriented Me$_2$-BPY layers. These results, shown in Figure 1d, reveal a lowering of the vacuum level above the SURMOF by 0.82 eV. This change directly translates into a core-level shift of atoms at the outer SURMOF surface. Overall, the simulations suggest a shift of 0.27 eV per polar layer for perfectly aligned dipoles (see the

Supporting Information). A quantitative comparison to the experimental data for a 70 cycle SURMOF with a thickness of 150 nm (corresponding to about 100 layers; see the Supporting Information) reveals that the experimentally observed change is substantially smaller.

To understand this deviation, we must consider in more detail the LbL process used to fabricate the SURMOFs. A perfect SURMOF, with the top layer consisting of Cu^{2+} paddlewheel units, exposes free axial sites. In the next deposition cycle, when the Me$_2$-BPY pillars are introduced, these will preferentially bind with their nonfunctionalized end (see Figure 1) to accessible surface Cu^{2+} ion, causing the molecular dipoles to be oriented away from the substrate. If this orientation is strictly maintained, the Cu^{2+} ions provided during the subsequent LbL step will coordinate to the opposite, methyl-substituted end of the Me$_2$-BPY, yielding a perfect NC structure. However, two factors might cause orientational defects. First, there is a chance that the asymmetric units simply bind with the "wrong" end. If an attachment via the functionalized and nonfunctionalized ends was to be equally probable, an up/down ratio of 1 would be expected, with no resulting net electric field and a quasi-centrosymmetric structure. Second, while in contact with the solvent, a "flipping" process of the Me$_2$-BPY unit might occur. Such flipping processes are unlikely to be triggered by lateral electrostatic interaction, since DFT calculations as well as electrostatic considerations reveal only small repulsive interactions

between adjacent linkers of less than 2 meV.[41] But, of course, entropic effects come into play, which also favor an up/down ratio of 1.

From the comparison of the experimental shifts in binding energy to the theoretical results, we conclude that the up/down ratio amounts to 1.07, i.e., 52% of the asymmetric bipyridine linkers exhibit an upward and 48% exhibit a downward orientation. Thus, although the overall impact on the electronic structure of the SURMOF is substantial, there is still plenty of room for improvements in the SURMOF fabrication process to achieve higher alignment ratios, including screening of solvents and optimizing fabrication temperatures.

Since a preferential orientation of the asymmetric Me_2-BPY removes the centrosymmetry of the symmetric Cu(BPDC)(BPY) SURMOF, the asymmetric thin film should also exhibit second-order NLO properties. While the generation of odd-numbered harmonics has been observed for numerous MOF materials (with a particularly strong third-order harmonic generation[39,40,49]), the observation of even-order harmonics is not possible for centrosymmetric compounds. Although the observation of SHG has been reported for a small number of MOF powder materials,[39] this interesting feature has not yet been seen for MOF thin films.

In Figure 1f, we show the optical response of a Cu(BPDC)(Me_2-BPY) SURMOF grown on (0001)-oriented sapphire substrates (see the Supporting Information for preparation details) when irradiated with light at 1064 nm and a pulse duration of 28 ps. A pronounced SHG signal at 532 nm can be clearly observed. Control experiments for the corresponding Sym SURMOFs, Cu(BPDC)(BPY), showed a strongly reduced, by an order of magnitude, SHG signal. The small, residual peak at 532 nm seen for the Sym SURMOF is attributed to surface SHG occurring at the MOF/air interface. These observations unambiguously demonstrate that the Cu(BPDC)(Me_2-BPY) SURMOF grown with the asymmetric linkers must exhibit a substantial fraction with an NC structure, in full accord with the shift of the Br 3d core levels.

To investigate the role of orientational defects on the SHG signal, we estimated the optical response of our asymmetric SURMOFs by computing the response functions connected to SHG (first (quadratic) hyperpolarizability $\beta_{ijk}(-2\omega, \omega, \omega)$). As a first step, we considered a single asymmetric Me_2-BPY chromophore, the NLO active elements of the MOFs (for details see the Supporting Information). From these molecular properties we then estimated the macroscopic second-order susceptibilities (χ_{IJK} and d_{IJK}) of the crystalline SURMOF thin films. The highest susceptibility (for a fully aligned sample) amounts to $d_{25} = -0.057$ pm V^{-1}, which is a factor of 25 lower than urea (1.4 pm V^{-1})[50] and an order of magnitude lower than that of second-order NLO organic crystal of KDP.[50]

For investigating the role of orientational defects, calculation was also carried out for a large supercell consisting of 1000 ($10 \times 10 \times 10$) unit cells with an up/down ratio of 1.07 (517/483, as estimated from the core-level shifts—vide supra). This gives a value of d_{25}(supercell) $= -0.002$ pm V^{-1}, a factor of ≈ 30 less than that for a perfectly aligned NC crystalline material. These results fully support the above interpretation of the SHG signal and demonstrate that recording SHG intensities is well suited to identify NC structures even in the absence of perfect ordering.

3. Conclusions

We have demonstrated a programmed LbL process to yield crystalline thin films of an NC structure with built-in electric fields. Using dipolar pillars as a basic unit, NC structures with integrated electric fields can be fabricated with shifts in the electrostatic potential up to 0.9 eV. Completely independent evidence for the NC nature of these MOF thin films is provided by the detection of a pronounced SHG signal. A theoretical analysis reveals that the observed NLO SHG efficiency is limited by the incomplete alignment of the dipolar building blocks. Thus, we see a distinct potential to further increase the first (quadratic) hyperpolarizability of asymmetric SURMOFs—and thus the total SHG efficiency—by further optimizing growth conditions to increase the degree of orientational order and by using pillars with larger, fully conjugated backbones.

The presence of tuneable, built-in electric fields opens up the possibility of engineering band structures and aligning electronic levels, in particular in connection with the loading of charge-donating guests (e.g., C_{60}[51]) into the pores of the SURMOFs.[52] In principle, the magnitude of the electrostatic potential shifts can be increased further—potentially even to the point where charge transfer from the substrate to the lowest unoccupied states at the outer SURMOF surface takes place. A further, highly promising route for future research is to orient asymmetric guests by embedding them into the pores of the NC SURMOFs, in which cases charge transfer might lead to further enhancement of the NLO properties. At present, the major obstacle hindering such further progress is the pronounced surface roughness and the high degree of orientational disorder in the SURMOFs. To overcome these limitations, in the future we will exploit automatized optimization of synthesis parameters using robot-based approaches to improve the structural quality of the NC SURMOFs.

Supporting Information

Supporting Information is available from the Wiley Online Library or from the author.

Conflict of Interest

The authors declare no conflict of interest.

Data Availability Statement

Research data are not shared.

Keywords

electrostatic design, metal–organic frameworks, second-harmonic generation

[1] J. Lu, X. Liu, M. Zhao, X. B. Deng, K. X. Shi, Q. R. Wu, L. Chen, L. M. Wu, *J. Am. Chem. Soc.* **2021**, *143*, 3647.

[2] G. D. Boyd, R. C. Miller, K. Nassau, W. L. Bond, A. Savage, *Appl. Phys. Lett.* **1964**, *5*, 234.

[3] W. J. Alford, A. V. Smith, *J. Opt. Soc. Am. B* **2001**, *18*, 524.

[4] R. A. McKee, F. J. Walker, M. F. Chisholm, *Phys. Rev. Lett.* **1998**, *81*, 3014.

[5] C. N. Ironside, in *Principles and Applications of Nonlinear Optical Materials* (Eds: R. W. Munn, C. N. Ironside), Springer Netherlands, Dordrecht, The Netherlands **1993**, p. 35.

[6] Z. H. Lim, N. F. Quackenbush, A. N. Penn, M. Chrysler, M. Bowden, Z. Zhu, J. M. Ablett, T. L. Lee, J. M. LeBeau, J. C. Woicik, P. V. Sushko, S. A. Chambers, J. H. Ngai, *Phys. Rev. Lett.* **2019**, *123*, 026805.

[7] J. C. Love, L. A. Estroff, J. K. Kriebel, R. G. Nuzzo, G. M. Whitesides, *Chem. Rev.* **2005**, *105*, 1103.

[8] M. Gärtner, E. Sauter, G. Nascimbeni, A. Wiesner, M. Kind, P. Werner, C. Schuch, T. Abu-Husein, A. Asyuda, J. W. Bats, M. Bolte, E. Zojer, A. Terfort, M. Zharnikov, *J. Phys. Chem. C* **2020**, *124*, 504.

[9] E. Ito, Y. Washizu, N. Hayashi, H. Ishii, N. Matsuie, K. Tsuboi, Y. Ouchi, Y. Harima, K. Yamashita, K. Seki, *J. Appl. Phys.* **2002**, *92*, 7306.

[10] P. Friederich, V. Rodin, F. von Wrochem, W. Wenzel, *ACS Appl. Mater. Interfaces* **2018**, *10*, 1881.

[11] F. Wurthner, *Acc. Chem. Res.* **2016**, *49*, 868.

[12] F. Wurthner, J. Schmidt, M. Stolte, R. Wortmann, *Angew. Chem., Int. Ed.* **2006**, *45*, 3842.

[13] W. M. K. P. Wijekoon, S. K. Wijaya, J. D. Bhawalkar, P. N. Prasad, T. L. Penner, N. J. Armstrong, M. C. Ezenyilimba, D. J. Williams, *J. Am. Chem. Soc.* **1996**, *118*, 4480.

[14] G. J. Ashwell, P. D. Jackson, W. A. Crossland, *Nature* **1994**, *368*, 438.

[15] W. Lin, W. Lin, G. K. Wong, T. J. Marks, *J. Am. Chem. Soc.* **1996**, *118*, 8034.

[16] M. J. Roberts, G. A. Lindsay, W. N. Herman, K. J. Wynne, *J. Am. Chem. Soc.* **1998**, *120*, 11202.

[17] A. Facchetti, A. Abbotto, L. Beverina, M. E. van der Boom, P. Dutta, G. Evmenenko, G. A. Pagani, T. J. Marks, *Chem. Mater.* **2003**, *15*, 1064.

[18] G. A. Neff, M. R. Helfrich, M. C. Clifton, C. J. Page, *Chem. Mater.* **2000**, *12*, 2363.

[19] M. E. van der Boom, A. G. Richter, J. E. Malinsky, P. A. Lee, N. R. Armstrong, P. Dutta, T. J. Marks, *Chem. Mater.* **2001**, *13*, 15.

[20] A. Facchetti, E. Annoni, L. Beverina, M. Morone, P. Zhu, T. J. Marks, G. A. Pagani, *Nat. Mater.* **2004**, *3*, 910.

[21] Y. Lu, Q. Gao, X. Yu, H. Zheng, R. Shen, Z. Hao, Y. Yan, P. Zhang, Y. Wen, G. Yang, S. Lin, *Research* **2020**, *2020*, 5714754.

[22] Y. Lin, C. Yang, S. Wu, X. Li, Y. Chen, W. L. Yang, *Adv. Funct. Mater.* **2020**, *30*, 2002918.

[23] R. Butté, N. Grandjean, in *Polarization Effects in Semiconductors: From Ab Initio Theory to Device Applications* (Eds: C. Wood, D. Jena), Springer US, Boston, MA, USA **2008**, pp. 467–511.

[24] B. Kretz, D. A. Egger, E. Zojer, *Adv. Sci.* **2015**, *2*, 1400016.

[25] V. Obersteiner, A. Jeindl, J. Gotz, A. Perveaux, O. T. Hofmann, E. Zojer, *Adv. Mater.* **2017**, *29*, 6.

[26] C. Winkler, S. S. Harivyasi, E. Zojer, *2D Mater.* **2018**, *5*, 035019.

[27] Y. Noguchi, W. Brutting, H. Ishii, *Jpn. J. Appl. Phys.* **2019**, *58*, SF0801.

[28] J. Kim, Y. S. Rim, Y. S. Liu, A. C. Serino, J. C. Thomas, H. J. Chen, Y. Yang, P. S. Weiss, *Nano Lett.* **2014**, *14*, 2946.

[29] D. Sheberla, J. C. Bachman, J. S. Elias, C. J. Sun, Y. Shao-Horn, M. Dinca, *Nat. Mater.* **2017**, *16*, 220.

[30] H. Furukawa, K. E. Cordova, M. O'Keeffe, O. M. Yaghi, *Science* **2013**, *341*, 1230444.

[31] S. Kitagawa, R. Kitaura, S.-I. Noro, *Angew. Chem., Int. Ed.* **2004**, *43*, 2334.

[32] O. Shekhah, H. Wang, S. Kowarik, F. Schreiber, M. Paulus, M. Tolan, C. Sternemann, F. Evers, D. Zacher, R. A. Fischer, C. Wöll, *J. Am. Chem. Soc.* **2007**, *129*, 15118.

[33] R. Haldar, C. Wöll, *Nano Res.* **2021**, *14*, 355.

[34] R. Haldar, L. Heinke, C. Wöll, *Adv. Mater.* **2020**, *32*, 1905227.

[35] A. M. Rice, C. R. Martin, V. A. Galitskiy, A. A. Berseneva, G. A. Leith, N. B. Shustova, *Chem. Rev.* **2020**, *120*, 8790.

[36] Z. Wang, J. Liu, S. Grosjean, D. Wagner, W. Guo, Z. Gu, L. Heinke, H. Gliemann, S. Bräse, C. Wöll, *ChemNanoMat* **2015**, *1*, 338.

[37] M. Drost, F. Tu, L. Berger, C. Preischl, W. Zhou, H. Gliemann, C. Wöll, H. Marbach, *ACS Nano* **2018**, *12*, 3825.

[38] M. Tu, B. Xia, D. E. Kravchenko, M. L. Tietze, A. J. Cruz, I. Stassen, T. Hauffman, J. Teyssandier, S. De Feyter, Z. Wang, R. A. Fischer, B. Marmiroli, H. Amenitsch, A. Torvisco, M. d. J. Velásquez-Hernández, P. Falcaro, R. Ameloot, *Nat. Mater.* **2021**, *20*, 93.

[39] C. Wang, T. Zhang, W. Lin, *Chem. Rev.* **2012**, *112*, 1084.

[40] Q. Wen, S. Tenenholtz, L. J. W. Shimon, O. Bar-Elli, L. M. Beck, L. Houben, S. R. Cohen, Y. Feldman, D. Oron, M. Lahav, M. E. van der Boom, *J. Am. Chem. Soc.* **2020**, *142*, 14210.

[41] G. Nascimbeni, C. Wöll, E. Zojer, *Nanomaterials* **2020**, *10*, 2420.

[42] K. Seki, W. Mori, *J. Phys. Chem. B* **2002**, *106*, 1380.

[43] A. Pichon, C. M. Fierro, M. Nieuwenhuyzen, S. L. James, *CrystEngComm* **2007**, *9*, 449.

[44] H. Chun, D. N. Dybtsev, H. Kim, K. Kim, *Chem. – Eur. J.* **2005**, *11*, 3521.

[45] Z. G. Gu, J. Burck, A. Bihlmeier, J. X. Liu, O. Shekhah, P. G. Weidler, C. Azucena, Z. B. Wang, S. Heissler, H. Gliemann, W. Klopper, A. S. Ulrich, C. Wöll, *Chem. – Eur. J.* **2014**, *20*, 9879.

[46] S. Porsgaard, P. Jiang, F. Borondics, S. Wendt, Z. Liu, H. Bluhm, F. Besenbacher, M. Salmeron, *Angew. Chem., Int. Ed.* **2011**, *50*, 2266.

[47] O. M. Cabarcos, A. Shaporenko, T. Weidner, S. Uppili, L. S. Dake, M. Zharnikov, D. L. Allara, *J. Phys. Chem. C* **2008**, *112*, 10842.

[48] T. C. Taucher, I. Hehn, O. T. Hofmann, M. Zharnikov, E. Zojer, *J. Phys. Chem. C* **2016**, *120*, 3428.

[49] C. Gu, H. Zhang, Y. You, Q. Zhang, G. Luo, Q. Shen, Z. Wang, J. Hu, *Nano Lett.* **2019**, *19*, 9095.

[50] A. Miniewicz, S. Bartkiewicz, E. Wojaczynska, T. Galica, R. Zalesny, R. Jakubas, *J. Mater. Chem. C* **2019**, *7*, 1255.

[51] X. J. Liu, M. Kozlowska, T. Okkali, D. Wagner, T. Higashino, G. Brenner-Weifss, S. M. Marschner, Z. H. Fu, Q. Zhang, H. Imahori, S. Brase, W. Wenzel, C. Wöll, L. Heinke, *Angew. Chem., Int. Ed.* **2019**, *58*, 9590.

[52] A. Chandresh, X. J. Liu, C. Wöll, L. Heinke, *Adv. Sci.* **2021**, *8*, 2001884.